Title

In vivo water state measurements in breast cancer using broadband diffuse optical spectroscopy

Journal

Physics in Medicine and Biology, 53(23)

ISSN

0031-9155

Authors

Chung, SH

Cerussi, AE

Klifa, C

et al.

Publication Date

2008-12-07

DOI

10.1088/0031-9155/53/23/005

Published in final edited form as:
Phys Med Biol. 2008 December 7; 53(23): 6713–6727. doi:10.1088/0031-9155/53/23/005.

In vivo water state measurements in breast cancer using broadband diffuse optical spectroscopy

S H Chung[1,2], **A E Cerussi**[1], **C Klifa**[3], **H M Baek**[4], **O Birgul**[4], **G Gulsen**[4], **S I Merritt**[5], **D Hsiang**[6], and **B J Tromberg**[1,2]

1 *Beckman Laser Institute, University of California, Irvine, 1002 Health Sciences Road, Irvine 92612, CA, USA*

2 *Department of Biomedical Engineering, University of California, Irvine, 3120 Natural Sciences II, Irvine, CA 92697-2715, USA*

3 *Magnetic Resonance Science Center, Radiology, University of California, San Francisco, 505 Parnassus Avenue, Box 0628, San Francisco, CA 94143-0628, USA*

4 *Tu and Yuen Center for Functional Onco Imaging, Department of Radiological Sciences, University of California, Irvine, 108 Irvine Hall, Irvine, CA, 92697-5020, USA*

5 *Masimo Corporation, 40 Parker, Irvine, CA 92618, USA*

6 *Department of Surgery, Chao Family Comprehensive Cancer Center, Univiersity of California, Irvine, Healthcare, 101 The City Drive South, Orange, CA 92868, USA*

Abstract

Structural changes in water molecules are related to physiological, anatomical and pathological properties of tissues. Near infrared (NIR) optical absorption methods are sensitive to water, however detailed characterization of water in thick tissues is difficult to achieve because subtle spectral shifts can be obscured by multiple light scattering. In the NIR, a water absorption peak is observed around 975nm. The precise NIR peak shape and position is highly sensitive to water molecular disposition. We introduce a Bound Water Index (BWI) that quantifies shifts observed in tissue water absorption spectra measured by broadband Diffuse Optical Spectroscopy (DOS). DOS quantitatively measures light absorption and scattering spectra and therefore reveals bound-water spectral shifts. BWI as a water state index was validated by comparing broadband DOS to Magnetic Resonance Spectroscopy, diffusion-weighted MRI and conductivity in bound water tissue phantoms. Non-invasive DOS measurements of malignant and normal breast tissues performed in 18 subjects showed a significantly higher fraction of free water in malignant tissues ($p<0.0001$) compared to normal tissues. BWI of breast cancer tissues inversely correlated with Nottingham-Bloom-Richardson histopathology scores. These results highlight broadband DOS sensitivity to molecular disposition of water, and demonstrate the potential of BWI as a non-invasive *in-vivo* index that correlates with tissue pathology.

1. Introduction

Approximately 60–80% of the human body is composed of water (Marieb, 1995). A variety of techniques including MRI, NMR and Diffuse Optical methods have been used to measure tissue water content in brain (Brooks *et al.*, 1989; Kreis *et al.*, 1993), breast (Cerussi *et al.*,

E-mail: bjtrombe@uci.edu.

2007; Jakubowski *et al.*, 2004; Pogue *et al.*, 2004), bone (Fantazzini *et al.*, 2001; Wang, 2003) and other tissues (Mathur-De Vre, 1984; Mirrashed and Sharp, 2004)

In addition to the volume fraction of water, water state can provide more detailed cellular and molecular information about tissues. Water mobility measurements using diffusion-weighted MRI (DW-MRI) and diffusion-tensor imaging have received considerable attention for their ability to measure cellularity and fiber orientation in brain and muscle tissues (Basser *et al.*, 1994; Hajnal *et al.*, 1991; Henkelman *et al.*, 1994; Mulkern *et al.*, 1999; Pierpaoli *et al.*, 1996). MRI also has demonstrated that diffusing free water mobility differs between tumor and normal tissues, and correlates inversely with cellularity (Guo *et al.*, 2002; Lyng *et al.*, 2000; Paran *et al.*, 2004). The low mobility of water in tumor tissues may be related to fractional changes in macromolecules, cellular membranes and intracellular components. However, the precise effect of microstructure on DW-MRI parameters is not well-understood (Mardor *et al.*, 2003; Thelwall *et al.*, 2002). Thus accurate measurements of bound water using DW-MRI are difficult to be obtained since macromolecules unbound to water as well as cell membranes bound to water present barriers to water diffusion (Callaghan *et al.*, 1993; Cho *et al.*, 1996; Nusbaum *et al.*, 2000; Putz *et al.*, 1992).

The goal of this research is to develop a new method that measures the molecular disposition of water in thick tissues by analyzing near infrared (NIR) absorption spectra. In previous work, we and others have demonstrated that Diffuse Optical methods can be used to measure increased water concentration in tumors relative to normal tissues (Cerussi *et al.*, 2007; Cerussi *et al.*, 2006; Jakubowski *et al.*, 2004; Paran *et al.*, 2004; Pogue *et al.*, 2004; Spinelli *et al.*, 2004). We have also shown that the optically-measured water concentration correlates with the Bloom-Richardson score of tumor histopathologic grade (Cerussi *et al.*, 2006). The bound water fraction measured by optical techniques can communicate water molecular vibrational states associated with macro molecular complexes in tissues (Brubach *et al.*, 2005; Eisenberg, 1969; Fisher *et al.*, 1970; Libnau *et al.*, 1994; Pimentel and McClellan, 1960; Scherems et al., 1984) and may provide additional insight regarding tissue pathophysiology. Because of increased binding of water to macromolecules such as proteins, the water absorption peak at 975nm undergoes both broadening and red shifting (Bellamy, 1968; Eisenberg, 1969; Pauling, 1960; Pimentel and McClellan, 1960). These spectral changes appear as a consequence of variations in the relative contributions of harmonic overtones from fundamental O-H vibrations at 3.05μm and 2.87μm (Eisenberg, 1969). In this work, we introduce a Bound Water Index (BWI) using these spectral changes obtained from scattering-corrected 650-998nm tissue absorption spectra measured by broadband Diffuse Optical Spectroscopy (DOS).

The sensitivity and accuracy of DOS to water state was validated by measuring bound water phantoms with controlled amounts of bound water. BWI, T2 relaxation times, conductivity and apparent diffusion coefficient (ADC) were measured and compared to BWI. Once established, BWI measurements were obtained from 18 patient volunteers with breast cancer. Breast tissue types were differentiated based on a significantly higher fraction of free water in malignant tissues compared to normal tissues ($p<0.0001$). Our clinical results also show that although there is significantly (~116%) increased water content in breast tumors, there is ~41% greater bound water fraction in normal vs. tumor containing breast. BWI was inversely correlated with Nottingham-Bloom-Richardson histopathology scores ($R = -0.96$) for all participating breast cancer patients. These findings are discussed in terms of underlying tumor-induced changes in cellularity and extracellular matrix and the potential for BWI to be used as prognostic indicator of tumor grade.

2. Methods

2.1. Instrumentation

The details of the broadband DOS system have been previously described (Bevilacqua *et al.*, 2000; Cerussi *et al.*, 2006). Broadband DOS combines multi frequency domain photon migration (FDPM) with broadband steady state (SS) spectroscopy. Multi-frequency FDPM separates the effects of absorption and scattering in tissues (Fishkin and Gratton, 1993; Tromberg *et al.*, 1993). Specifically, we have used a P1 approximation to the transport equation in the semi-infinite geometry using an extrapolated boundary condition (Fishkin *et al.*, 1996; Haskell *et al.*, 1994). The SS component enables the acquisition of continuous high resolution absorption spectra of more than 1000 wavelengths from 650 to 998nm, the upper spectral limit of our spectrometer (B&W Tek, *Newark, DE, model* 611a). Since the spectrometer is auto-calibrated, the absolute wavelength spectrum can be obtained for every measurement. Instrument response is determined using tissue-simulating phantoms for FDPM and spectraflect-coated integrating spheres for SS measurements with known scattering and absorption values as described in Cerussi et al. (Cerussi *et al.*, 2006).

Measurements are performed by placing a specially-designed handpiece onto the surface of the test material or subject. The multi-frequency (50~600MHz) swept FDPM data for 658, 682, 785, 810, 830 and 850nm lasers (<20mW power) and SS data for all wavelengths between 650 and 998nm are acquired in a total of ~ 6 seconds. The source-detector separation is 29mm for breast measurements and the interrogated tissue volume by DOS is approximately $10cm^3$. Model fits to SS and FDPM data were performed in order to recover absorption (μ_a) and reduced scattering (μ_s') values for all NIR wavelengths (650–998nm) as described in Bevilacqua et al. and Cerussi et al.

2.2. Tissue spectral processing

The extinction coefficient spectra of major tissue chromophores (oxy- and deoxy-hemoglobin, water and bulk lipid were used to recover tissue concentrations of these components (ctO_2Hb (μM), ctHHb (μM), ctH2O (%, a relative ratio to pure water concentration (55.6M)) and ctLipid (%, a relative value to pure lipid density of 0.9 $g \cdot ml^{-1}$), respectively) from tissue absorption spectra (Cerussi *et al.*, 2002 and 2007, Cubeddu *et al.*, 2000, Pogue *et al.*, 2004, Quaresima *et al.*, 1998)). For oxy- and deoxy-hemoglobin, we employed molar extinction coefficients of Zjilstra et al (Zijlistra, 2000). For water, we obtained extinction coefficients by measuring distilled water in a cuvette using a spectrophotometer (Beckman DU 650) at various temperatures in order to account for possible temperature effects (Merritt, 2005). The employed extinction coefficient values of lipid were obtained from mammalian fat by van Veen et al (van Veen et al., 2005). The tissue absorption spectrum and extinction coefficient spectra provided needed information to solve nonnegative least-squares constraints problems (using 'lsqnonneg' in MATLAB®) to recover the concentrations of the four principal NIR absorbers.

The tissue absorption spectra (figure 1(a) solid line) were post-processed to measure bound water state using a 3 step process. First, a tissue water spectrum ($\mu_{a,\ tissue\ water}$) was obtained by eliminating non-water tissue absorbers' contributions by subtracting the extinction coefficient spectra of oxy- and deoxy- hemoglobin and bulk lipid multiplied by the concentration of each tissue chromophore (obtained using the method described above) from the overall tissue absorption spectrum. Second, the residual between the tissue ($\mu_{a,\ tissue\ water}$) and pure water spectra ($\mu_{a,\ pure\ water}$) was calculated by subtracting the pure water spectrum (at physiological temperature, 36°C for breast tissues (Jeffrey *et al.*, 1999)) from a normalized tissue water spectrum in the wavelength range from 935nm to 998nm. Finally, in order to represent the residual using an index, the absolute values of the differences

were combined and divided by the number of points in the sum to form the Bound Water Index (BWI) (figure 1, equation (1)).

$$BWI = \frac{\sum_i \left| \frac{\mu_{a,\text{tissue water}}(\lambda_i)}{ctH_2O} - \mu_{a,\text{pure water}}(\lambda_i) \right|}{N} \times 1000 \quad (1)$$

where λ_i is i^{th} wavelength (935nm $\leq \lambda_i \leq$ 998nm), ctH_2O is the water concentration described above and N is the number of wavelength points in the sum. 935nm was chosen because above 935nm the tissue water absorption spectrum is linearly shifted to higher wavelengths relative to the pure water spectrum (Merritt, 2005).

We have investigated the effect of the temperature of the pure water spectrum used in the second step above. It is possible that the temperature could vary depending on the status of the tissue, personal difference, room temperature etc. We measured the temperature dependent NIR absorption spectra of pure water between 15 and 65 °C. We then simulated the potential impact of physiological temperature fluctuations by using water reference spectra obtained from 34°C to 38°C. Our results showed that BWI varied by up to 4% with temperature fluctuations in this range (data not shown). Since the simulation demonstrates that the effect on BWI would be small, we chose one temperature (36°C), previously measured for in vivo breast tissue (Jeffrey *et al.*, 1999), for all in-vivo BWI calculations

2.3. Turbid thick tissue phantom measurements

The accuracy of DOS bound water measurements was tested using bound water phantoms with varying bound water fractions. Measurements were compared to 2 gold standard methods: Magnetic Resonance Spectroscopy and conductivity. Diffusion-weighted MRI was also used to characterize the apparent diffusion coefficient of each phantom.

2.3.1. Phantom fabrication—Different concentrations of bound water phantoms were made by mixing varying amounts of gelatin powder (0, 8, 16 and 20g for figure 2 and 4, and 0, 6, 9,15 and 21g for figure 3) from porcine skin (G2500-1KG, Sigma-Aldrich) with intralipid (Liposyn II, 20%, Abbott Laboratories), nigrosin (Sigma-Aldrich) and distilled water. The gelatin powders, 30ml intralipid, 1.5ml nigrosin (511mg/1L stock solution) were dissolved in 300ml water at 37°C and incubated at 37°C while stirred with a magnetic stir bar for 22–24 hours. Then the fully dissolved phantoms were cooled and hardened in a cold room at 5–7°C for 22–24 hours (te Nijenhuis, 1997).

2.3.2. Broadband DOS phantom measurements and spectral processing—All phantoms were measured in semi-infinite geometry three times using broadband DOS with a source-detector separation of 21.5mm. BWI for phantoms was calculated in the same manner as for tissue (described in section 2.2). However, unlike tissue, phantoms do not contain hemoglobin and the main phantom spectral components are a composite of water, lipid, and nigrosin contributions. Consequently, a phantom water spectrum was obtained by subtracting the complementary phantom spectral components, (i.e. lipid and nigrosin) from the composite phantom spectrum. The employed extinction coefficient spectrum of nigrosin was measured in a cuvette using a spectrophotometer. The resulting phantom water spectra were compared to pure water spectra (at the corresponding temperature) in order to obtain phantom BWI. The temperature of the phantoms was measured before and after each measurement using a thermistor. This allowed us to correct for possible temperature effects in phantoms and measure water spectral changes only due to the bound water.

2.3.3. Magnetic Resonance Spectroscopy phantom measurements—Proton MR spectroscopy (MRS) was performed on a 3.0T (e.g., 127 MHz) scanner (Achieva; Philips Medical System, Cleveland, Ohio) with a birdcage head coil. Axial images using a T1-weighted spin echo sequence (repetition time (TR)/echo time (TE) = 1100/12 ms) was used for placing the volume of interest (VOI) in the phantoms before MRS. The voxel size was $2 \times 2 \times 2$ cm^3 in the phantom. For localization, MRS spectra were obtained using a point-resolved spin-echo sequence (PRESS) (Bottomley, 1987). Shimming was performed automatically on the water resonance for the optimization of homogeneity in each VOI. A fully relaxed, unsuppressed spectrum (e.g., 32 averages and 1024 data points) was acquired in order to measure the amplitude of the water peak in the localized volume. For data analysis, no line broadening was applied before Fourier transformation. Manual zero and first-order phase corrections without baseline correction were applied and water peak integration was performed on processed spectra using jMRUI (Naressi et al., 2001) version 3.0 package.

For the T2 relaxation time measurement, TR of 2000 ms and TE of 60, 120, 240, 480 and 960 ms were used. The T2 values of water were calculated using the following equation

$$M_s = M_0 \times \left(e^{-TE/T2}\right) \quad (2)$$

where M_s denotes the signal intensity of the measurement at a given TE and M_0 denotes the signal where TE = 0.

The T2 relaxation time with increasing gelatin concentration was fit to a mono-exponential curve. A mono-exponential decay with increasing protein amount is expected from a two-state model with rapid exchange between bound and bulk water in phantoms with protein (Fukuzaki *et al.*, 1995; Lambelet *et al.*, 1988; Moser *et al.*, 1996; Oakes, 1976a). The relationship between T2 relaxation rate (R2 = 1/T2) and BWI was also investigated since a linear relationship between the proton relaxation rate and protein concentration is predicted in this model.

2.3.4. Conductivity measurement of the phantoms using a conductivity measurement cell—A four electrode conductivity measurement cell was employed to measure bound water phantom conductivity. Gelatin was hardened inside the conductivity cell for its complete contact to each electrode. After the current was measured at both longitudinal ends of the conductivity cell, the current was used to calculate electrical resistance of the gelatin using two electrodes in the middle of the cell. Then, the conductivity of the phantom was calculated by dividing the length between the two electrodes in the middle by the electrical resistance times cross sectional area of the cell. ($\sigma = l/(R \cdot A)$, σ: conductivity, l: length between the two electrodes in the middle, R: electrical resistance of the gelatin, A: area of the cell). Each phantom was measured two times.

2.3.5. Apparent Diffusion Coefficient measurements of the bound water phantoms—The ADC of water is obtained from diffusion weighted MRI, an imaging technique that measures the mobility of water in tissues and is sensitive to such parameters as cell organization and microstructure. Details of the technical approach for diffusion weighted MRI used in this research are reported in the paper of Patridge et al (Partridge et al., 2001). Images were acquired using a 1.5T GE Signa scanner (GE Medical Systems, Milwaukee, WI) with a bilateral phased-array breast coil (MRI Devices Corp., Waukesha, WI). Employed imaging parameters were TE 49.5 ms, TR 5348 ms, flip angle 90°, 0.5 NEX (number of excitations), 6-mm slice thickness, pixel size 1.56 × 1.56 × 6mm, and a 128 × 128 acquisition matrix. Diffusion weighting factor (b value) used for the data in figure 4 was b= 400 seconds/mm^2. Diffusion weighted images were fit on a pixel-by-pixel basis to equation (3).

$$S = S_0 \times e^{-b \times ADC} \quad (3)$$

Equation (3) relates the decrease in signal intensity observed with increasing *b*-factor or ADC where S and S_0 are the signal intensities in each pixel with and without diffusion weighting.

2.4. Patient measurements

Broadband DOS measurements were acquired from 18 subjects who had infiltrating ductal carcinoma (IDC, N=16) and infiltrating lobular carcinoma (N=2). The mean subject age was 51 ± 9.6 with a range of 37 to 65. The average tumor size, which was taken to be the maximum tumor dimension, was 35±24 mm, with a range of 13 to 100 mm. Linear reflectance linescans were performed in all subjects both over the region of the tumor and in the same location on the contralateral normal side. The details of the linescan have been described in Cerussi et al (Cerussi et al., 2006). The linescan location was chosen based upon *a priori* knowledge of the tumor location from standard X-ray mammography or ultrasound. We assumed that the contralateral side of the lesion breast was normal tissue unless otherwise indicated in the final pathology report. Linescans were performed with 10-mm increments using a source–detector separation of 29 mm. We kept the handheld probe contact gentle and constant as much as possible. In related studies we examined the impact of probe contact pressure on our measurements. BWI varied 1.2±0.8% (N=3 subjects) when the normal contact pressure was increased by 50% (data not shown). This pressure difference required substantial force and is significantly higher than the pressure applied during patient measurements. Consequently, under normal use conditions, the impact of probe pressure variation on BWI is expected to be negligible.

In order to compare normal and malignant tissues, we calculated an average value of a measured parameter from all locations on a line on the normal breast and an average value of three continuous peak points of BWI on the malignant tumor on the contralateral lesion breast.

3. Results

3.1. BWI measurements on phantoms

The BWI of bound water phantoms with various amounts of gelatin were measured (figure 2). BWI increased linearly with gelatin concentration (R=0.98). Each phantom was measured three times on slightly different locations, and the measurement variation in BWI is also plotted. The offset of BWI at 0g gelatin concentration is likely due to water bound to intralipid components.

Phantoms made by the same fabrication method were measured with MRS and conductivity cell in order to validate the DOS-measured bound water dependence in the bound water phantoms. The T2 relaxation times are shown in figure 3 (a). The water peak (127.8 MHz) was broader in bound water phantoms than a liquid intralipid phantom without gelatin (not shown). As the gelatin concentration increased, the T2 relaxation times decreased with R^2=0.996. Each T2 relaxation time was measured once per phantom. Similar trends have been observed by Fukuzaki et al (Fukuzaki et al., 1995) who showed exponential decreases of T2 relaxation times as the amount of albumin increased. The relationship between T2 relaxation rate and BWI is shown on figure 3 (c). R2 had high correlation with BWI (R=0.96).

The conductivity of each bound water phantom was measured twice using a four electrode conductivity measurement cell as described in 2.3.4. The conductivity increased linearly as the gelatin concentration increased (R=0.95) as shown in figure 3(b). The BWI and conductivity of the phantoms had a high linear correlation (R=0.99) (figure 3(d)).

The ADC of water from the bound water phantoms was compared to BWI (figure 4). The phantoms in figure 2 were measured after 10 days using diffusion-weighted MRI as described in 2.3.5. An inverse linear correlation between the ADC and BWI (R=−0.97) was obtained. We confirmed that the BWI of the phantoms did not change significantly after 10 days (2.25 ±1.3%). This result suggests that the degree of water molecule diffusion decreased with increasing protein-water binding.

3.2. In vivo breast tissue measurements

In figure 5, TOI and BWI of both lesion and normal breasts of one of the IDC patients are depicted. This patient (57 years old, post-menopausal) had a 4 × 3.5cm tumor on her left breast according to ultrasound. On the lesion side, the TOI values were higher and the BWI values were lower than the normal side. The higher TOI is due to elevated concentrations of water and deoxy-hemoglobin and reduced lipid in tumor tissues. This trend was found in all 18 subjects. The average value of two (for tumor less than 2cm) or three (for tumor bigger than 2cm) continuous BWI peak points in the window in figure 5 was used to calculate BWI of tumor tissues, and it coincides with the location of the lesion. In general, the TOI and BWI values represent an average measurement of tumor and normal tissues of the measured tissue volume (Cerussi *et al.*, 2006).

BWI values from malignant (1.96±0.3) and normal tissues (2.77±0.47) in 18 subjects compared using the Wilcoxon ranked-sum test (figure 6) were significantly different ($p<0.0001$). Malignant tumors had lower BWI than normal tissues, suggesting that tumors appear to have more free than bound water. The relationship between bulk water concentration and BWI of normal and malignant tissues was also studied (figure 7). In general, BWI is inversely proportional to tissue water content. In normal tissues, the water content range is relatively narrow (10~28%) and the BWI spans between 2.3 and 4.3. However, in cancer tissues, the bulk water content values are high and widely spread (22~73%) while the BWI is clustered between 1.4 and 2.4.

Based on previous findings that correlate water content with histopathological grade (Cerussi *et al.*, 2006), figure 7 suggests that BWI may provide additional insight into tumor invasiveness. In order to explore this relationship further, we examined the Nottingham-Bloom-Richardson scores (Nottingham scores) of breast cancer tissues. The Nottingham-Bloom-Richardson grading system uses objective criteria to assess three main features; tubule formation, nuclear pleomorphism and mitotic count. A histopathologic grade is given on a relative scale of 3–9, where 9 corresponds to the highest grade tumor.

Figure 8 shows that the BWI decreased with increasing Nottingham score (R=−0.96, p=0.002). The black squares are the average values of BWI for each score. There was only one subject for Nottingham score 3. The solid line represents a linear fit to the data points.

4. Discussion

We developed an optical bound water index (BWI) from quantitative tissue absorption spectra in the NIR. In order to validate the accuracy and sensitivity of BWI for water state measurements, bound water phantoms were fabricated and tested using MRS and a conductivity measurement cell.

Figure 2 demonstrates that BWI increases linearly with phantom gelatin content (R=0.98). Since gelatin fraction was the only variable in all phantoms, we conclude that BWI measures water disposition changes caused by gelatin.

In order to confirm that the phantoms indeed have protein bound water, each was measured using MRS and a conductivity measurement cell. T2 relaxation time is strongly affected by the number of water binding sites in tissue (Fullerton and Dornbluth, 1982; Moser *et al.*, 1996). Many studies have shown the ability of T2 for measuring water mobility in biological tissues such as breast, brain and lung (Assaf *et al.*, 1997; Brauer, 2003; Shioya *et al.*, 1997; Tan *et al.*, 2008). The T2 value increases as freely mobile water increases. In figure 3(a), T2 relaxation time decreased mono-exponentially as protein concentration increased. This result is due to reduced excitation of nuclei in bound states and consequent fast recovery. Also the mono-exponential decrease of T2 values satisfies a two-state model with a rapid exchange between the bound and bulk water (Fukuzaki *et al.*, 1995; Lambelet *et al.*, 1988; Moser *et al.*, 1996; Oakes, 1976a). T2 values smaller than T1 relaxation times (less than half of T2 values, not shown) signify the prevalence of heterogeneous water-proton environments in our phantoms, which is associated with bound water molecules (Odajima, 1959; Sasaki et al., 1960). High correlation between T2 relaxation rates (R2) and protein concentration has been reported in other studies (Lambelet *et al.*, 1988; Moser *et al.*, 1996; Oakes, 1976a) which is also from the two-state model. Thus, the high correlation between R2 and BWI (figure 3(c)) suggests that BWI measures macromolecular bound water accurately.

Careri *et al*. have observed increasing conductivity with increasing bound water fraction as shown in figure 3(b). By analyzing the relationship between dielectric constant and conductivity, they found that the protons involved in the conductivity at 100kHz are not the free hydrogen ions of the solvent, but the ions bound to ionizable groups of proteins (Careri et al., 1985). The high correlation between BWI and conductivity shown in figure 3(d) further demonstrates the reliability of BWI as an index for bound water fraction.

DW-MRI has been used to measure water state in *in-vivo* tissues using apparent diffusion coefficients (ADC) of water. In figure 4, ADC and BWI from homogeneous phantoms demonstrated an inverse correlation suggesting that as more water is bound to macromolecules the degree of water diffusion decreases. Based on our clinical data where the BWI decreased in tumor tissues (figure 5 and 6), this would suggest that ADC and BWI are complementary and ADC should increase in tumors. Interestingly, previous MRI studies have demonstrated lower ADC in malignant tumors compared to both normal tissue and benign tumors (Englander et al., 1997;Guo et al., 2002;Partridge et al., 2001). However, in these studies the ADC is typically measured on regions of interest (ROI) carefully drawn to exclude necrotic and cystic areas. If any of the necrotic, cystic or fat regions are included, ADC values change significantly. Paran et al.(Paran et al., 2004) acquired heterogeneous diffusion parameters on large, progressing tumors due to partial and full necrotic loci spread throughout the tumor tissues. It is challenging to select an ROI that only represents the cellular part of a tumor due to the low resolution of DW-MRI images. In addition, the diffusion of free water can be obstructed by the presence of macromolecules and fibrous structures unbound to water (Callaghan et al., 1993;Cho et al., 1996;Nusbaum et al., 2000;Putz et al., 1992). Thus, the interpretation of bound water state in tissues using ADC will vary substantially depending on tissue micro-structure and the precise ROI selected. In contrast, BWI represents an average bulk property of the tissue and is a relatively simple measurement to acquire and interpret.

In normal well-differentiated tissues, we expect a relatively narrow range of BWI and water content values due to the absence of significant disorder and the expectation that normal tissues have an intrinsic maximum water content and binding capacity (figure 7). With the appearance of cancer and loss of differentiation, water content increases dramatically and the tissue structural diversity increases. This phenomenon is communicated by the wide range of water content values and reductions in BWI seen in figure 7.

Overall, significantly lower BWI was observed in tumor vs. normal tissues (figure 5–7). This indicates that the water associated with tumor tissues is more like free water. This could be from necrotic regions in the tumors where free water can fill. The measured free water increase might also be related to alterations in extracellular matrix (ECM). Hyaluronan (or, hyaluronic acid, HA), one of the components of the ECM, is a large, negatively charged polysaccharide that participates in transducing signals in proliferating and migrating cells, and it is closely related to tumor growth (Vignal *et al.*, 2002), metastasis (Hayen et al., 1999), increased drug resistance (Baumgartner et al., 1998), cellular invasiveness (Toole, 2001) and angiogenesis in malignant tumors.(West et al., 1985) In breast cancer patients, high levels of HA in the stroma are associated with low survival rate (Auvinen et al., 2000;Vignal et al., 2002). HA has the ability to retain water and the meshwork structure exerts swelling pressure because of increased mutual repulsion between and within HA molecules (Toole, 2004). Therefore, the figure 8 finding that water binding state correlates inversely with tumor histopathological grade maybe related to the increased presence of HA and necrotic regions in malignant tumors. This inverse correlation between BWI and tumor grade complements our previous observation that overall water content positively correlates with histopathological scores (Cerussi et al., 2006). BWI appears to convey additional information about tissue pathological changes specifically related to the molecular disposition of water, possibly due to alterations in cellularity and extracellular matrix. Although preliminary, these results suggest that both water content and disposition as measured by DOS may provide clinical prognostic information related to metastatic potential and therapeutic outcome

In conclusion, we provide evidence that water state is communicated effectively by the optical measurement of BWI. The accuracy of BWI as a water state index has been validated in bound water phantoms by comparing broadband DOS to MRS and a conductivity measurement cell. Breast cancers were found to possess significantly more free than bound water and BWI correlated inversely with tumor histopathological grade. These results highlight broadband DOS sensitivity to tissue water content and state, and underscore the potential for BWI to be used as a complementary index to MRI relaxation time and ADC measurements.

Acknowledgements

This work was supported by the National Institutes of Health under Grants P41-RR01192 (Laser Microbeam and Medical Program: LAMMP) and U54-CA105480 (Network for Translational Research in Optical Imaging: NTROI); and the Chao Family Comprehensive Cancer Center (P30-CA62203). This work was also supported by programmatic support by Beckman Foundation and Medical Free Electron Laser program (MFEL). Early part of this work was also supported by International Research Internship program by the Korea Science and Engineering Foundation (KOSEF) and the Korea Research Foundation (M07-2004-000-10161-0). The authors thank the patients who cheerfully volunteered to participate in this study. We also thank Montana Compton for her assistance with organizing the clinical trial. So Hyun Chung also thanks Chris Raub for the help for finding the bound water phantom recipe. We specially thank Dr. Enrico Gratton for the discussion related to this research.

References

Assaf Y, BeitYannai E, Shohami E, Berman E, Cohen Y. Diffusion- and T-2-weighted MRI of closed-head injury in rats: A time course study and correlation with histology. Magnetic Resonance Imaging 1997;15:77–85. [PubMed: 9084028]

Auvinen P, et al. Hyaluronan in peritumoral stroma and malignant cells associates with breast cancer spreading andpredicts survival. Am J Pathol 2000;156:529–36. [PubMed: 10666382]

Basser PJ, Mattiello J, Lebihan D. MR Diffusion tensor spectroscopy and imaging. Biophysical Journal 1994;66:259–67. [PubMed: 8130344]

Baumgartner G, et al. The impact of extracellular matrix on the chemoresistance of solid tumors — experimental and clinical results of hyaluronidase as additive to cytostatic chemotherapy. Cancer Lett 1998;131:85–99. [PubMed: 9839623]

Bellamy, LJ. Advances in Infrared Group Frequencies. London: Chapman and Hall; 1968.

Bevilacqua F, Berger AJ, Cerussi AE, Jakubowski D, Tromberg BJ. Broadband absorption spectroscopy in turbid media by combined frequency-domain and steady-state methods. Applied Optics 2000;39:6498–507. [PubMed: 18354663]

Bottomley PA. Spatial localization in NMR spectroscopy in vivo. Ann N Y Acad Sci 1987;508:333–48. [PubMed: 3326459]

Brauer M. In vivo monitoring of apoptosis. Progress in Neuro-Psychopharmacology & Biological Psychiatry 2003;27:323–31. [PubMed: 12657370]

Brooks DJ, Luthert P, Gadian D, Marsden CD. Does signal-attenuation on high-field T2-weighted MRI of the brain reflect regional cerebral iron deposition - observations on the relationship between regional cerebral water proton T2 values and iron levels. Journal of Neurology Neurosurgery and Psychiatry 1989;52:108–11.

Brubach JB, Mermet A, Filabozzi A, Gerschel A, Roy P. Signatures of the hydrogen bonding in the infrared bands of water. Journal of Chemical Physics 2005;122:184509. [PubMed: 15918731]

Callaghan PT, Coy A, Forde LC, Rofe CJ. Diffusive relaxation and edge enhancement in NMR microscopy. Journal of Magnetic Resonance Series A 1993;101:347–50.

Careri G, et al. Protonic conductivity of hydrated lysozyme powders at megahertz frequeccies. PNAS 1985;82:5342–6. [PubMed: 3860864]

Cerussi, et al. Spectroscopy enhances the information content of optical mammography. Journal of Biomedical Optics 2002;7:60–71. [PubMed: 11818013]

Cerussi A, Hsiang D, Shah N, Mehta R, Durkin A, Butler J, Tromberg BJ. Predicting response to breast cancer neoadjuvant chemotherapy using diffuse optical spectroscopy. Proceedings of the National Academy of Sciences of the United States of America 2007;104:4014–9. [PubMed: 17360469]

Cerussi A, Shah N, Hsiang D, Durkin A, Butler J, Tromberg BJ. In vivo absorption, scattering, and physiologic properties of 58 malignant breast tumors determined by broadband diffuse optical spectroscopy. Journal of Biomedical Optics 2006;11:044005. [PubMed: 16965162]

Cho ZH, Hong IK, Ro YM. Some new observations on pulse sequence dependent diffusion related edge enhancement in MR microscopy. Magnetic Resonance in Medicine 1996;36:197–203. [PubMed: 8843372]

Cubeddu R, et al. Effects of the menstrual cycle on the red and near-infrared optical properties of the human breast. Photochem Photobiol 2000;72:383–391. [PubMed: 10989610]

Eisenberg, D.; Kauzmann, W. The Structure and Properties of Water. Oxford: Clarendon Press; 1969.

Englander SA, et al. Diffusion imaging of human breast. NMR Biomed 1997;10:348–52. [PubMed: 9471126]

Fantazzini P, Viola R, Alnaimi SM, Strange JH. Combined MR-relaxation and MR-cryoporometry in the study of bone microstructure. Magnetic Resonance Imaging 2001;19:481–4. [PubMed: 11445335]

Fisher HF, McCabe WC, Subraman S. Near-infrared spectroscopic investigation of effect of temperature on structure of Water. Journal of Physical Chemistry 1970;74:4360–9.

Fishkin JB, Fantini S, VandeVen MJ, Gratton E. Gigahertz photon density waves in a turbid medium: Theory and experiments. Physical Review E 1996;53:2307–19.

Fishkin JB, Gratton E. Propagation of photon-density waves in strongly scattering media containing an absorbing semiinfinite plane bounded by a straight edge. Journal of the Optical Society of America a-Optics Image Science and Vision 1993;10:127–40.

Fukuzaki M, Miura N, Shinyashiki N, Kurita D, Shioya S, Haida M, Mashimo S. Comparison of water relaxation-time in serum-albumin solution using nuclear-magnetic-resonance and time-domain reflectometry. Journal of Physical Chemistry 1995;99:431–5.

Fullerton GDPJ, Dornbluth NC. NMR relaxation of protons in tissue and ohter macromolecular water solutions. Magnetic Resonance Imaging 1982;1:209–28. [PubMed: 6927208]

Guo Y, Cai YQ, Cai ZL, Gao YG, An NY, Ma L, Mahankali S, Gao JH. Differentiation of clinically benign and malignant breast lesions using diffusion-weighted imaging. Journal of Magnetic Resonance Imaging 2002;16:172–8. [PubMed: 12203765]

Hajnal JV, Doran M, Hall AS, Collins AG, Oatridge A, Pennock JM, Young IR, Bydder GM. MR imaging of anisotropically restricted diffusion of water in the nervous-system - technical, anatomic, and

pathological considerations. Journal of Computer Assisted Tomography 1991;15:1–18. [PubMed: 1987175]

Haskell RC, Svaasand LO, Tsay TT, Feng TC, Mcadams MS. Boundary-conditions for the diffusion equation in radiative-transfer. Journal of the Optical Society of America a-Optics Image Science and Vision 1994;11:2727–41.

Hayen W, Goebeler M, Kumar S, Riessen R, Nehls V. Hyaluronan stimulates tumor cell migration by modulating the fibrin fiber architecture. Journal of Cell Science 1999;112:2241–51. [PubMed: 10362554]

Henkelman RM, Stanisz GJ, Kim JK, Bronskill MJ. Anisotropy of NMR properties of tissues. Magnetic Resonance in Medicine 1994;32:592–601. [PubMed: 7808260]

Jakubowski DB, Cerussi AE, Bevilacqua F, Shah N, Hsiang D, Butler J, Tromberg BJ. Monitoring neoadjuvant chemotherapy in breast cancer using quantitative diffuse optical spectroscopy: a case study. Journal of Biomedical Optics 2004;9:230–8. [PubMed: 14715078]

Jeffrey SS, Birdwell RL, Ikeda DM, Daniel BL, Nowels KW, Dirbas FM, Griffey SM. Radiofrequency ablation of breast cancer - First report of an emerging technology. Archives of Surgery 1999;134:1064–8. [PubMed: 10522847]

Kreis R, Ernst T, Ross BD. Development of the Human Brain - in-Vivo Quantification of Metabolite and Water-Content with Proton Magnetic-Resonance Spectroscopy. Magnetic Resonance in Medicine 1993;30:424–37. [PubMed: 8255190]

Lambelet P, Berrocal R, Desarzens C, Froehlicher I, Ducret F. Pulsed Low-Resolution Nmr Investigations of Protein Sols and Gels. Journal of Food Science 1988;53:943–6.

Libnau FO, Kvalheim OM, Christy AA, Toft J. Spectra of Water in the Nearinfrared and Midinfrared Region. Vibrational Spectroscopy 1994;7:243–54.

Lyng H, Haraldseth O, Rofstad EK. Measurement of cell density and necrotic fraction in human melanoma xenografts by diffusion weighted magnetic resonance imaging. Magnetic Resonance in Medicine 2000;43:828–36. [PubMed: 10861877]

Mardor Y, Pfeffer R, Spiegelmann R, Roth Y, Maier SE, Nissim O, Berger R, Glicksman A, Baram J, Orenstein A, Cohen JS, Tichler T. Early detection of response to radiation therapy in patients with brain malignancies using conventional and high b-value diffusion-weighted magnetic resonance imaging. Journal of Clinical Oncology 2003;21:1094–100. [PubMed: 12637476]

Marieb, EN. Human Anatomy and Physiology. Redwood City, California: Benjamin/Cummings; 1995.

Mathur-De Vre R. Biomedical implications of the relaxation behaviour of water related to NMR imaging. The British Journal of Radiology 1984;57:955–76. [PubMed: 6100168]

Merritt, SI. PhD thesis Physics. University of California; Irvine: 2005. Combination of broadband diffuse optical spectroscopy with magnetic resonance imaging.

Mirrashed F, Sharp JC. In vivo morphological characterisation of skin by MRI micro-imaging methods. Skin Research and Technology 2004;10:149–60. [PubMed: 15225264]

Moser E, Holzmueller P, Krssak M. Improved estimation of tissue hydration and bound water fraction in rat liver tissue. Magnetic Resonance Materials in Physics Biology and Medicine 1996;4:55–9.

Mulkern RV, Gudbjartsson H, Westin CF, Zengingonul HP, Gartner W, Guttmann CRG, Robertson RL, Kyriakos W, Schwartz R, Holtzman D, Jolesz FA, Maier SE. Multi-component apparent diffusion coefficients in human brain. NMR in Biomedicine 1999;12:51–62. [PubMed: 10195330]

Naressi A, Couturier C, Devos JM, Janssen M, Mangeat C, de Beer R, Graveron-Demilly D. Java-based graphical user interface for the MRUI quantitation package. Magnetic Resonance Materials in Physics Biology and Medicine 2001;12:141–52.

Nusbaum AO, Lu DF, Tang CY, Atlas SW. Quantitative diffusion measurements in focal multiple sclerosis lesions: Correlations with appearance on TI-weighted MR images. American Journal of Roentgenology 2000;175:821–5. [PubMed: 10954474]

Oakes J. Protein Hydration. J Chem Soc Faraday I 1976a;72:216–27.

Odajima A. Nuclear magnetic resonance studies of water sorbed on fibrous materials. Journal of the Physical Society of Japan 1959;14:308–12.

Paran Y, et al. Water diffusion in the different microenvironments of breast cancer. NMR Biomed 2004;17:170–80. [PubMed: 15229930]

Partridge SC, et al. Menstrual cycle variation of apparent diffusion coefficients measured in the normal breast using MRI. Journal of Magnetic Resonance Imaging 2001;14:433–8. [PubMed: 11599068]

Pauling, L. The nature of the chemical bond. Ithaca, New York: Cornell University Press; 1960.

Pierpaoli C, Jezzard P, Basser PJ, Barnett A, DiChiro G. Diffusion tensor MR imaging of the human brain. Radiology 1996;201:637–48. [PubMed: 8939209]

Pimentel, GC.; McClellan, AL. The Hydrogen Bond. San Francisco: W. H. Freeman and Company; 1960.

Pogue BW, Jiang SD, Dehghani H, Kogel C, Soho S, Srinivasan S, Song XM, Tosteson TD, Poplack SP, Paulsen KD. Characterization of hemoglobin, water, and NIR scattering in breast tissue: Analysis of intersubject variability and menstrual cycle changes. Journal of Biomedical Optics 2004;9:541–52. [PubMed: 15189092]

Putz B, Barsky D, Schulten K. Edge Enhancement by Diffusion in Microscopic Magnetic-Resonance-Imaging. Journal of Magnetic Resonance 1992;97:27–53.

Quaresima V, Matcher SJ, Ferrari M. Identification and quantification of intrinsic optical contrast for near-infrared mammography. Photochem Photobiol 1998;67:4–14. [PubMed: 9477760]

Sasaki M, Kawai T, Hirai A, Hashi T, Odajima A. A Study of sorbed water on cellulose by pulsed NMR technique. Journal of the Physical Society of Japan 1960;15:1652–7.

Scherems O, et al. Hydrogen Bonding in Low-Temperature Matrices: 1. Proton donor abilities of fluoroalcohols. Comparative infrared studies of ROH```O(CH3)2 complex formation in the gas phase, in CCl4 solution, and in solid argon. J Phys Chem 1984;88:4335–42.

Shioya S, Tsuji C, Kurita D, Katoh H, Tsuda M, Haida M, Kawana A, Ohta Y. Early damage to lung tissue after irradiation detected by the magnetic resonance T-2 relaxation time. Radiation Research 1997;148:359–64. [PubMed: 9339952]

Spinelli L, Torricelli A, Pifferi A, Taroni P, Danesini GM, Cubeddu R. Bulk optical properties and tissue components in the female breast from multiwavelength time-resolved optical mammography. Journal of Biomedical Optics 2004;9:1137–42. [PubMed: 15568933]

Tan PC, Pickles MD, Lowry M, Manton DJ, Turnbull LW. Lesion T-2 relaxation times and volumes predict the response of malignant breast lesions to neoadjuvant chemotherapy. Magnetic Resonance Imaging 2008;26:26–34. [PubMed: 17573224]

te Nijenhuis K. Thermo reversible networks. Viscoelastic properties and structure of gels. Adv Polym Sci 1997;130:160–93.

Thelwall PE, Grant SC, Stanisz GJ, Blackband SJ. Human erythrocyte ghosts: Exploring the origins of multiexponential water diffusion in a model biological tissue with magnetic resonance. Magnetic Resonance in Medicine 2002;48:649–57. [PubMed: 12353282]

Toole BP. Hyaluronan in morphogenesis. Semin Cell Dev Biol 2001;12:79–87. [PubMed: 11292373]

Toole BP. Hyaluronan: From extracellular glue to pericellular cue. Nature Reviews Cancer 2004;4:528–39.

Tromberg BJ, Svaasand LO, Tsay TT, Haskell RC. Properties ofphoton density Waves in multiple-scattering media. Applied Optics 1993;32:607–16.

van Veen RLP, et al. Determination of visible near-IR absorption coefficients of mammalian fat using time- and spatially resolved diffuse reflectance and transmission spectroscopy. Journal of Biomedical Optics 2005;10:054004. [PubMed: 16292964]

Vignal P, Meslet MR, Romeo JM, Feuilhade F. Sonographic morphology of infiltrating breast carcinoma - Relationship with the shape of the hyaluronan extracellular matrix. Journal of Ultrasound in Medicine 2002;21:531–8.

Wang, XaNQ. Determination of cortical bone poreosity and pore size distibution using a low field pulsed NMR approach. Journal of Orthopaedic Reasearch 2003;21:312–9.

West DC, Hampson IN, Arnold F, Kumar S. Angiogenesis Induced by Degradation Products of Hyaluronic-Acid. Science 1985;228:1324–6. [PubMed: 2408340]

Zijlistra, WGea. Visible and Near Infrared Absorption Spectra of Human and Animal Haemoglobin: Determination and Application. Utrecht, The Netherlands: VSP; 2000.

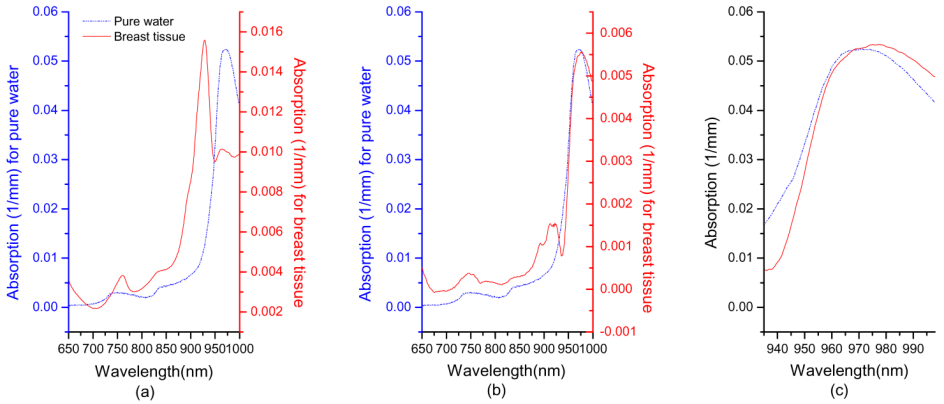

Figure 1.

(a) In vivo tissue absorption spectrum (solid line) from normal breast tissue. (b) Tissue water spectrum after subtracting other tissue components' spectra (solid line). (c) Normalized tissue water spectrum at 935-998nm (solid line). The pure water spectrum at 36°C is shown in each panel (a, b and c, dashed lines) for comparison.

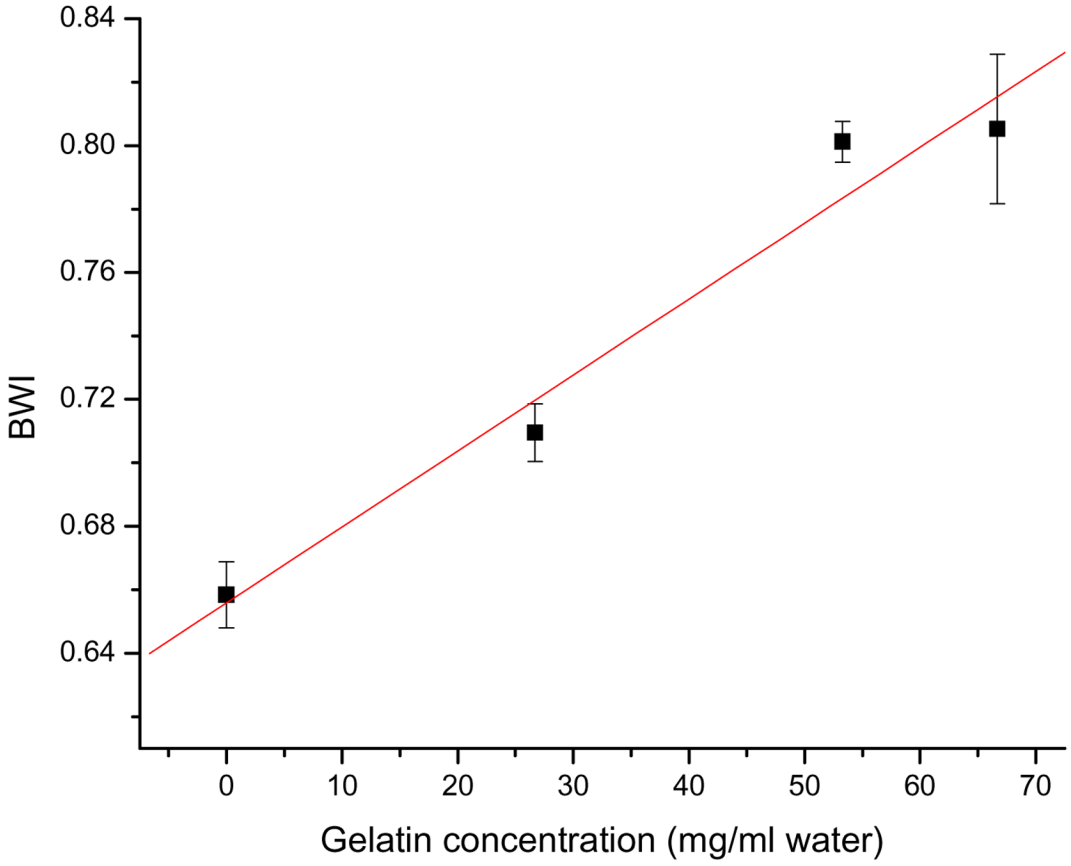

Figure 2.
BWI of bound water phantoms (linear fit, R=0.98, p=0.02). Error bars represent the differences between three measurements on the phantoms.

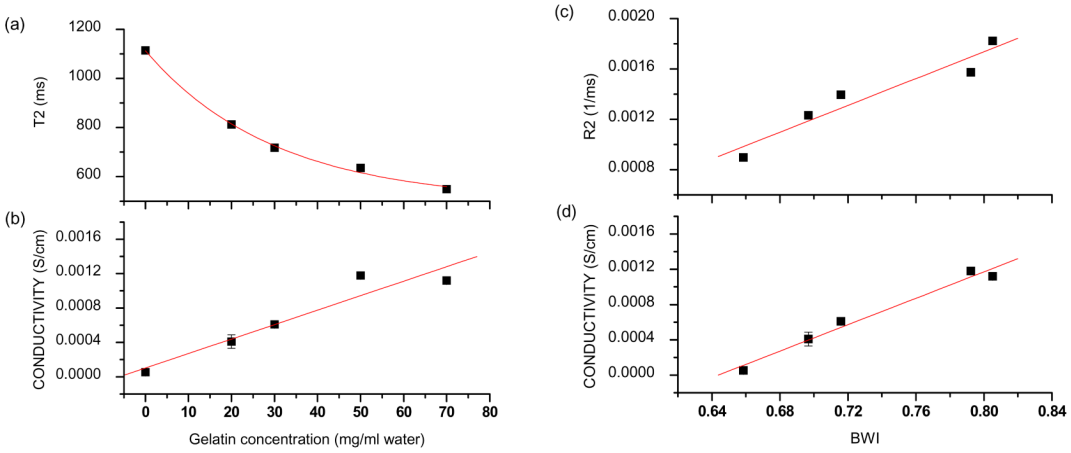

Figure 3.

T2 relaxation time/rate and conductivity of the phantoms. (a) T2 relaxation times vs. gelatin concentration (R^2=0.996, T2 values were measured one time per phantom). (b) Conductivity vs. gelatin concentrations (R=0.95, measured at 100kHz). (c) R2 vs. BWI (R=0.96) (d) Conductivity vs. BWI (R=0.99) Error bars represent the differences between two measurements on the phantoms (most of them are smaller than the symbol size).

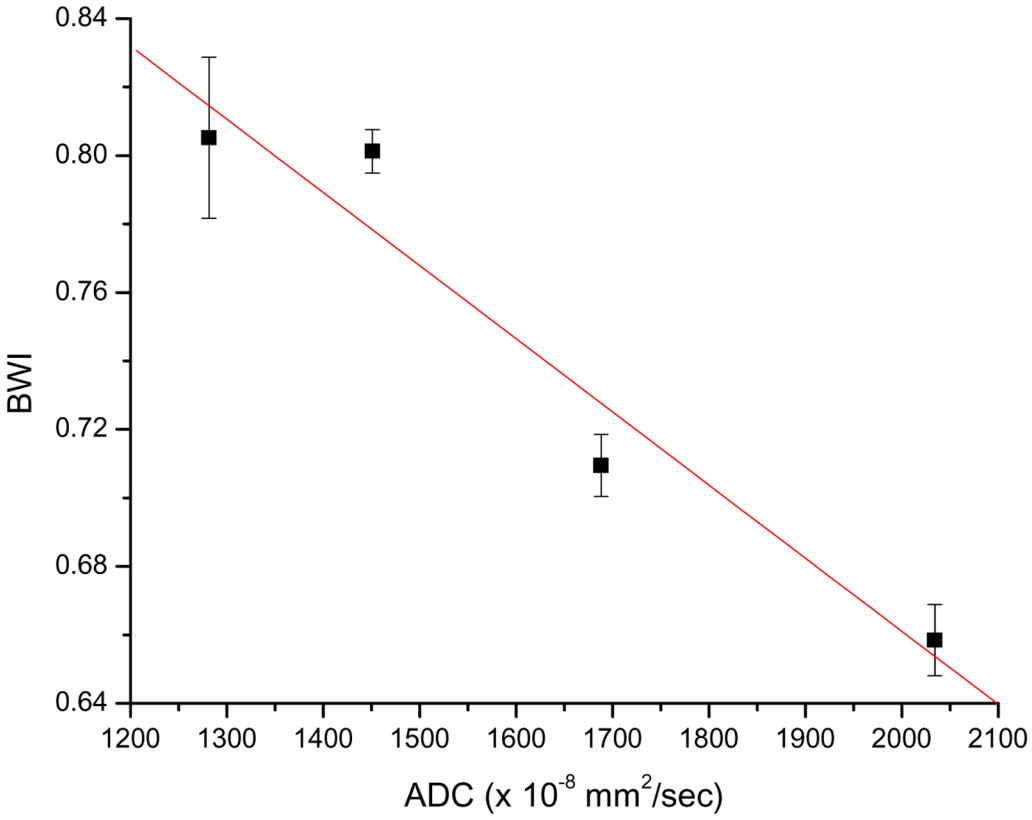

Figure 4.
BWI vs. ADC of water of bound water phantoms (R=−0.97). Error bars represent the differences between three measurements on the phantoms.

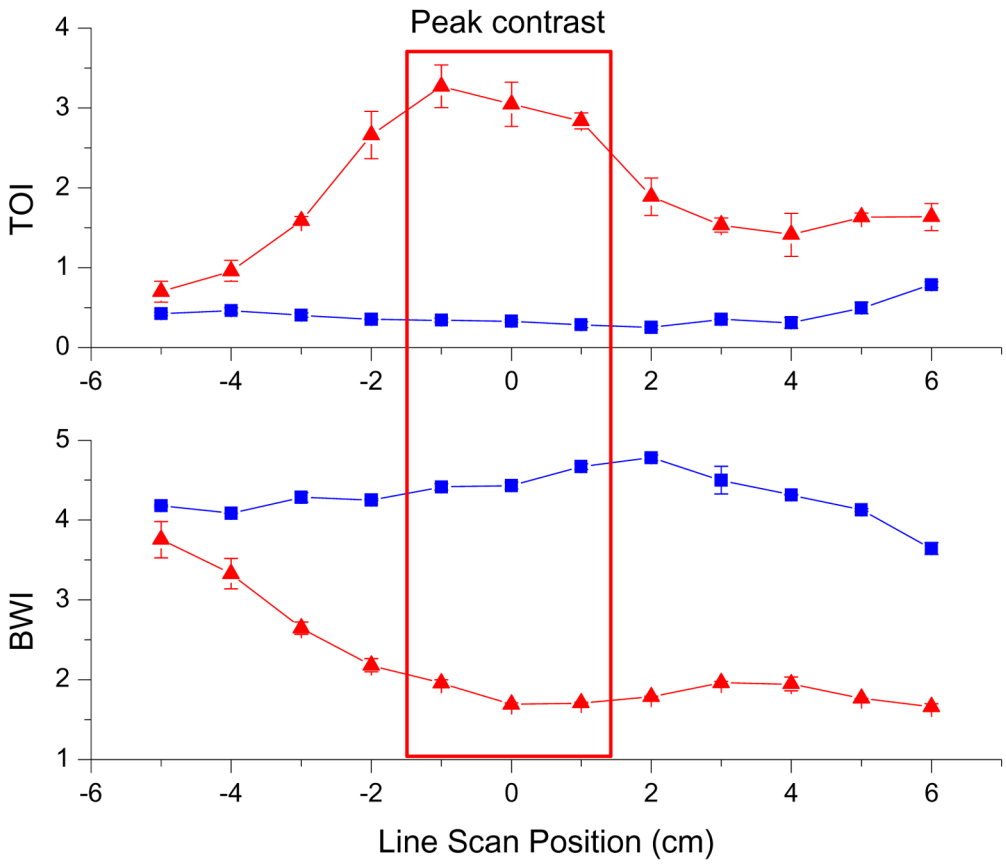

Figure 5.

Line scanned Tissue Optical Index (TOI = ctH_2O × ctHHb/ctLipid) and Bound Water Index (BWI) of normal (blue squares) and malignant breast tissues (red triangles). TOI is higher and BWI is lower in malignant tissues with respect to normal tissues. Three continuous peak points of the malignant tissues are highlighted.

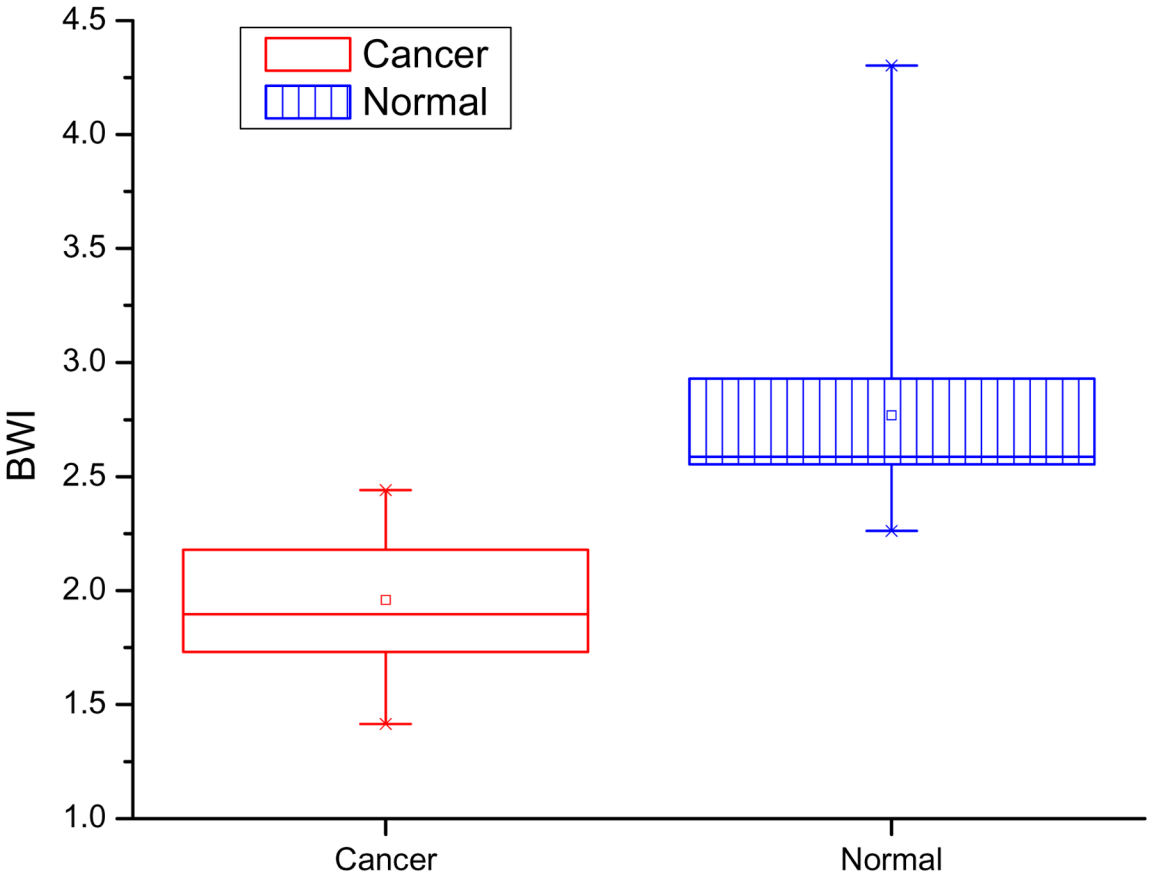

Figure 6.
Box plots of BWI of malignant (1.96±0.3) and normal breast tissues (2.77±0.47) for 18 subjects. Tumor and normal tissues were differentiated with statistical significance with $p<0.0001$ (Wilcoxon ranked-sum test).

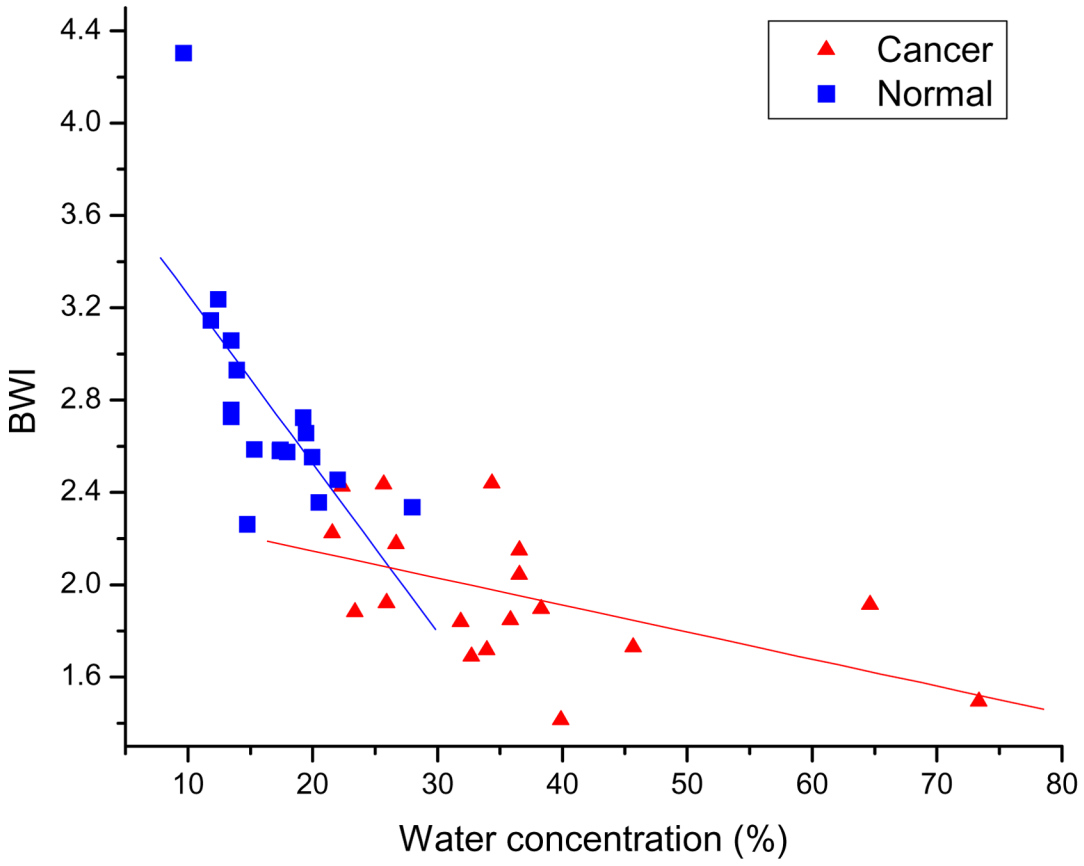

Figure 7.
BWI vs. bulk water concentration of normal (blue squares) and malignant (red triangles) breast tissues. Both bulk water concentrations and BWI values were acquired from the same spatial locations. Normal and malignant tissue groups were discriminated by two separate linear fittings with $\text{slope}_{\text{normal}} = -0.07 \pm 0.02$, and $\text{slope}_{\text{malignant}} = -0.01$.

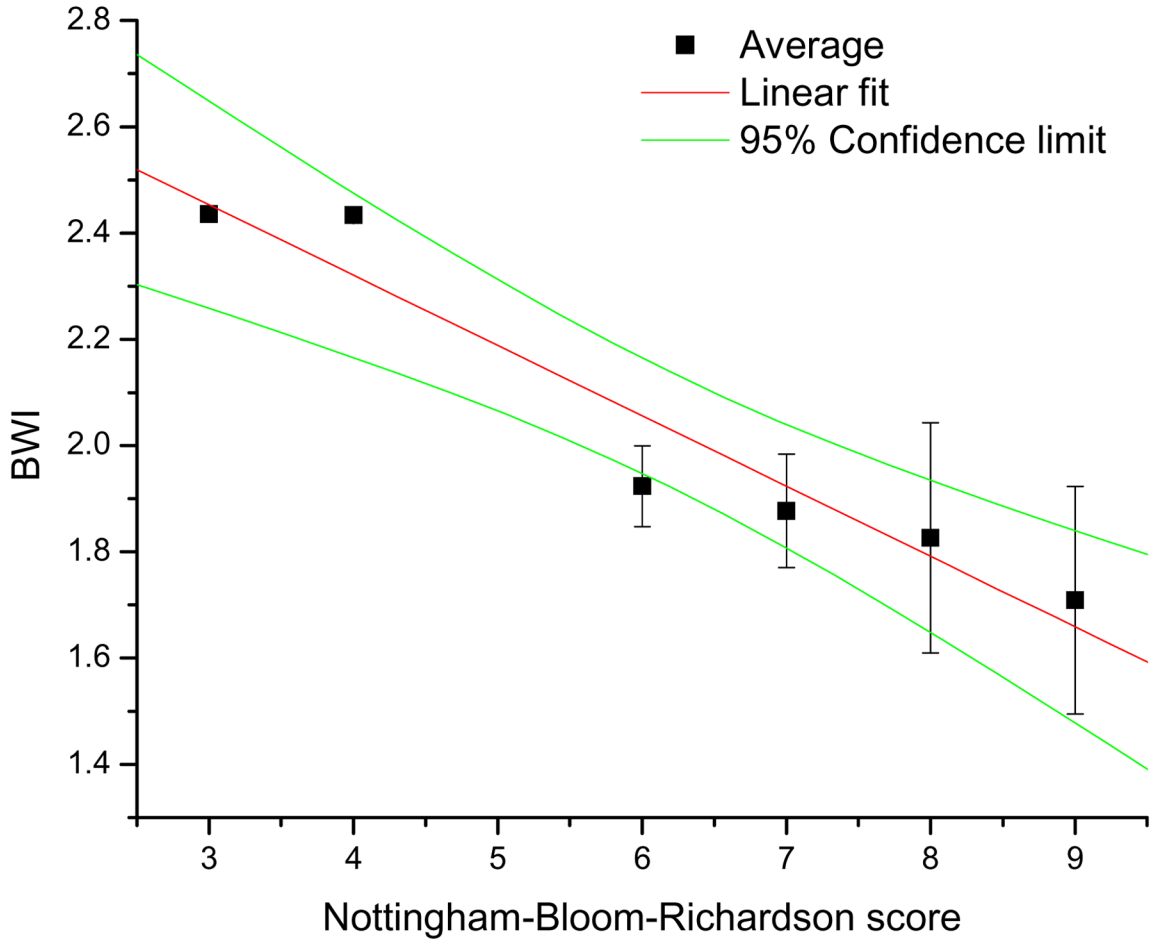

Figure 8.
BWI vs. Nottingham-Bloom-Richardson score. The average and standard deviation of BWI values of breast cancer tissue samples from 18 patients are depicted with black squares and error bars. The linear fit had R= −0.96.